Low-temperature properties of $Pb(Zr_{1-x}Ti_x)O_3$ solid solutions near the morphotropic phase boundary

L. Bellaiche[1], Alberto García[2] and David Vanderbilt[3]
[1] *Physics Department, University of Arkansas, Fayetteville, Arkansas 72701, USA*
[2] *Departamento de Fisica Aplicada II, Universidad del Pais Vasco, Apartado 644, 48080 Bilbao, Spain*
[3] *Center for Materials Theory, Department of Physics and Astronomy, Rutgers University, Piscataway, New Jersey 08855-0849, USA*

(February 14, 2001)

A first-principles-derived approach is used to study structural, piezoelectric and dielectric properties of $Pb(Zr_{1-x}Ti_x)O_3$ (PZT) solid solutions near the morphotropic phase boundary at low temperature. Three ferroelectric phases are found to exist: a tetragonal phase for larger x compositions, a rhombohedral phase for smaller x compositions, and the recently discovered monoclinic phase in between. In this monoclinic phase, the polarization associated with the Zr atoms behaves differently from the polarization associated with the Ti atoms. As the composition x decreases, the former rotates more quickly towards the pseudo-cubic [111] direction and grows in magnitude, while the latter lags in its rotation and its magnitude shrinks. The local microscopic structure is found to deviate significantly from the average structure in these PZT alloy phases as a result of fluctuations in the directions and magnitudes of the local polarizations. The monoclinic phase is characterized by a very large piezoelectric and dielectric response.

Keywords: Macroscopic phases, Local structure, Piezoelectricity, Dielectric response
PACS:77.84.Dy,77.65.Bn,77.22.Ch

I. INTRODUCTION

Since the beginning of the 70's, $Pb(Zr_{1-x}Ti_x)O_3$ (PZT) alloys have been known to exhibit a morphotropic phase boundary (MPB) separating a ferroelectric region with a tetragonal ground state ($x > 0.52$) from a ferroelectric region with rhombohedral symmetry ($x < 0.45$)[1]. Very recently, synchrotron x-ray powder diffraction studies have revealed that there is in fact a third phase in the vicinity of the MPB at low temperature[2]. This phase is ferroelectric, adopts a monoclinic symmetry and occurs within a narrow range of composition x that separates the tetragonal region from the rhombohedral region[2,3]. It has been suggested that this monoclinic phase acts as a transitional bridge between the tetragonal phase, for which the electrical polarization **P** lies along the pseudo-cubic [001] direction, and the rhombohedral phase, for which **P** is along the pseudo-cubic [111] direction[2]. The use of a recently developed first-principles approach has confirmed that this is indeed the case, since the polarization of the monoclinic phase has been found to rotate from the [001] to the [111] direction as the composition x decreases in the MPB region[4].

Despite these experimental and theoretical advances, some features related to this MPB are still unknown. For instance, one may wonder what is the separate contribution of Zr and Ti atoms to the rotation of the polarization in this monoclinic phase. One may also want to know if the local (microscopic) structure of a PZT alloy near its MPB differs strongly from its average (macroscopic) structure, as suggested by Ref. 3.

Moreover, PZT is strongly piezoelectric in the vicinity of the MPB[5], which is a primary reason why these materials are of current use in transducers and other piezoelectric devices[6]. Recent theoretical and experimental work has reexamined the piezoelectricity of tetragonal and rhombohedral PZT alloys[4,7]. However, we are not aware of any previous studies of the piezoelectric or dielectric response in the monoclinic phase of PZT.

The purpose of the present article is to apply the newly-developed first-principles derived scheme of Ref. 4 to PZT and to investigate all the issues mentioned above. Our main findings are as follows. (1) As the Ti composition decreases in the recently discovered monoclinic phase, the polarization associated with Zr atoms rotates towards the [111] direction and grows in magnitude, while the polarization associated with Ti atoms lags in its rotation toward this [111] direction and shrinks in magnitude. (2) There are strong fluctuations of the direction and magnitude of the local polarizations centered in the different unit cells of PZT alloys near the MPB, indicating that various unit cells adopt a local structure somewhat different from the macroscopic average. (3) The recently discovered monoclinic phase exhibits very large piezoelectric and dielectric coefficients.

The paper is organized as follows. In Sec. II, we describe our approach in detail. Section III reports our results, and we conclude in Sec. IV.

II. METHODS

We use the numerical scheme proposed in Ref. 4, which consists of constructing an alloy effective Hamiltonian from first-principles calculations. For a *ferroelectric* material, the effective Hamiltonian should include structural degrees of freedom corresponding to the ferroelectric local soft mode and the strain variables. These are the most important degrees of freedom because ferroelectric transitions are accompanied by a softening of the phonon soft mode and by the appearance of a strain[8]. Moreover, a realistic *alloy* effective Hamiltonian must also include the compositional degrees of freedom, because the atomic arrangement can strongly affect the ferroelectric properties of an alloy[9]. We proposed to incorporate all such degrees of freedom by writing the total energy E as a sum of two energies,

$$E(\{\mathbf{u}_i\},\{\mathbf{v}_i\},\eta_H\{\sigma_j\}) = E_{\text{ave}}(\{\mathbf{u}_i\},\{\mathbf{v}_i\},\eta_H) + E_{\text{loc}}(\{\mathbf{u}_i\},\{\mathbf{v}_i\},\{\sigma_j\}) \ , \quad (1)$$

where $\mathbf{u}_i$ is the local B-centered soft mode in unit cell i of the ABO_3 perovskite material under study; $\{\mathbf{v}_i\}$ are the dimensionless local displacements which are related to the inhomogeneous strain variables inside each cell and which are centered on the A-sites[8]; η_H is the homogeneous strain tensor; and the $\{\sigma_j\}$ characterize the atomic configuration of the alloy. That is, σ_j=+1 or −1 corresponds to the presence of a Zr or Ti atom, respectively, at the B-sublattice site j of the $Pb(Zr_{1-x}Ti_x)O_3$ solid solution. The energy E_{ave} depends only on the soft-mode and strain variables. The $\{\sigma_j\}$ parameters are incorporated into the second energy term E_{loc}, which thus accounts for the chemical differences between Zr and Ti atoms.

Expressions for the total energy E have recently been proposed[8,10] for *simple* ABO_3 perovskite systems (i.e., in the absence of $\{\sigma_j\}$ variables). These have been very successful both for reproducing phase transition sequences[8,10,11] and for studying ferroelectric domain walls[12], as well as for calculating finite-temperature dielectric and electromechanical properties[13–15]. Here, for E_{ave}, we generalized the analytical expression of Ref. 8 to the case of the $Pb(Zr_{1-x}Ti_x)O_3$ alloy, by making use of the virtual crystal approximation (VCA)[16–18]. We thus replaced the $Pb(Zr_{1-x}Ti_x)O_3$ alloy by a virtual (uniform) $Pb\langle B\rangle O_3$ simple system in which the ⟨B⟩ atom is a virtual atom involving a kind of potential average between Zr and Ti atoms[17]. E_{ave} thus consists of five parts: a local-mode self-energy, a long-range dipole-dipole interaction, a short-range interaction between soft modes, an elastic energy, and an interaction between the local modes and local strain[8]. The analytical expression for E_{ave} has 18 free parameters that are determined by fitting to the results of almost 40 first-principles calculations on small VCA cells (typically between 5 and 20 atoms/cell) following the procedure of Ref. 8. More precisely, the first-principles method used is the plane-wave ultrasoft-pseudopotential method[19] within the local-density approximation (LDA)[20], and the VCA approach adopted is the one of Ref. 17. Table I reports the resulting 18 expansion parameters of E_{ave} for the $Pb(Zr_{0.5}Ti_{0.5})O_3$ alloy.

TABLE I. Expansion parameters (in atomic units) of E_{ave} for $Pb(Zr_{0.5}Ti_{0.5})O_3$.

Parameter	Value
κ_2	0.0138
α	0.011
γ	0.002
j_1	−0.00577
j_2	0.01425
j_3	0.00140
j_4	−0.00094
j_5	0.00141
j_6	0.00006
j_7	0.00003
B_{11}	5.22
B_{12}	1.67
B_{44}	1.22
B_{1xx}	−0.374
B_{1yy}	−0.155
B_{4yz}	−0.068
Z^*	7.342
ϵ_∞	7.150

While expressions were available for E_{ave}, we were not aware of any analytical expression that had previously been proposed and tested for E_{loc}. Following the spirit of the "computational alchemy" method developed for calculating the compositional energy of semiconductor alloys[21–23], we derived E_{loc} by treating the alloy configuration $\{\sigma_j\}$ as a perturbation of the VCA system. We adopted an expression that includes: (i) the *on-site* effect of alloying on the self-energy up to the fourth order in the local mode amplitude $\mathbf{u}_i$; and (ii) the *intersite* contributions involving the first-order terms in a perturbation expansion in powers of σ_j (i.e., terms that are linear in $\mathbf{u}_i$ or $\mathbf{v}_i$). That is,

$$E_{\text{loc}}(\{\mathbf{u}_i\},\{\mathbf{v}_i\},\{\sigma_j\}) = \sum_i [\Delta\alpha(\sigma_i)\ u_i^4 \ + \ \Delta\gamma(\sigma_i)\ (u_{ix}^2 u_{iy}^2 + u_{iy}^2 u_{iz}^2 + u_{iz}^2 u_{ix}^2)] + \sum_{ij} [Q_{|j-i|}\ \sigma_j\ \mathbf{e}_{ji}\cdot\mathbf{u}_i \ + \ R_{|j-i|}\ \sigma_j\ \mathbf{f}_{ji}\cdot\mathbf{v}_i] \ , \quad (2)$$

where the sum over i runs over all the unit cells, while the sum over j runs over the mixed sublattice sites. u_{ix}, u_{iy} and u_{iz} are the Cartesian coordinates of the local-mode $\mathbf{u}_i$. $\mathbf{e}_{ji}$ is a unit vector joining the site j to the center of the soft mode $\mathbf{u}_i$, and $\mathbf{f}_{ji}$ is a unit vector joining the site j to the origin of $\mathbf{v}_i$. $\Delta\alpha(\sigma_i)$ and $\Delta\gamma(\sigma_i)$ characterize the on-site contribution of alloying. Their strength and sign reflect how the identity of the atom sitting on the i site affects the local-mode self energy of the "VCA" $Pb(Zr_{1-x}Ti_x)O_3$ solid solution. $Q_{|j-i|}$ and $R_{|j-i|}$ are related to intersite interactions between the alloy parameter σ_j on the site j and the local mode u_i and the strain-related v_i at the site i, respectively. $Q_{|j-i|}$ and $R_{|j-i|}$ only depend on the distance between i and j up to the third neighbors shell, while for symmetry reasons, the expression for the intersite interactions becomes more complex when going beyond the third neighbors shell. In principle, terms involving higher powers of $\{\sigma_j\}$, $\mathbf{u}_i$ and $\mathbf{v}_i$ might be included to improve the quality of the expansion, but as shown in Ref. 4, we found this level of expansion to give a very good account of experimental findings. We also found that $Q_{|j-i|}$ and $R_{|j-i|}$ rapidly decrease as the distance between i and j increases. As a result, we included the contribution up to the third neighbors for $Q_{|j-i|}$ (denoted Q_1, Q_2 and Q_3 in the following) and up to the first neighbor shell for $R_{|j-i|}$ (denoted R_1).

The parameters $\Delta\alpha(\sigma_i)$, $\Delta\gamma(\sigma_i)$, $Q_{|j-i|}$ and $R_{|j-i|}$ are also derived by performing first-principles calculations, and are given in Table II in the case of the $Pb(Zr_{0.5}Ti_{0.5})O_3$ alloy. More precisely, $\Delta\alpha(\sigma_i)$ and $\Delta\gamma(\sigma_i)$ are derived by computing the energy of a 5-atom cell containing a true B-atom [e.g., Ti or Zr in $Pb(Zr,Ti)O_3$] when the atoms are displaced as in the VCA local mode. Then $Q_{|j-i|}$ and $R_{|j-i|}$ are derived by using large ideal cubic cells (up to 40 atoms) containing a central true B-atom surrounded by VCA atoms, and are simply related to the atomic forces occurring on these VCA atoms.

TABLE II. Expansion parameters of $E_{\rm loc}$ (in atomic units) for $Pb(Zr_{0.5}Ti_{0.5})O_3$. σ=+1 and -1 corresponds to the presence of a Zr and Ti atom, respectively.

Parameter	Value
$\Delta\alpha(+1)$	0.003
$\Delta\alpha(-1)$	−0.003
$\Delta\gamma(+1)$	−0.010
$\Delta\gamma(-1)$	0.003
Q_1	0.00160
Q_2	−0.00028
Q_3	−0.00018
R_1	−0.0125

In principle, all the parameters in Eqs. (1) and (2) should change when one varies the composition x in the $Pb(Zr_{1-x}Ti_x)O_3$ solid solution. However, we assumed that only the parameters related to the local-mode self-energy – i.e., α and γ for the VCA alloy, and $\Delta\alpha(\sigma_i)$ and $\Delta\gamma(\sigma_i)$ in Eq (2) – can significantly change with composition. This composition-dependence was assumed to be linear, and was determined by performing first-principles simulations on cells with two different compositions, namely x=0.5 and x = 0.45. The resulting composition-dependencies are

$$
\begin{aligned}
\alpha + \Delta\alpha(+1) &= 0.014 + 0.02\,(0.5-x) \\
\alpha + \Delta\alpha(-1) &= 0.008 + 0.02\,(0.5-x) \\
\gamma + \Delta\gamma(+1) &= -0.008 - 0.14\,(0.5-x) \\
\gamma + \Delta\gamma(-1) &= 0.005 - 0.02\,(0.5-x)
\end{aligned}
\tag{3}
$$

Such a linear composition-dependence approach is only realistic when exploring a narrow range of compositions, as done in Ref. 4 and in the present study.

Once our effective Hamiltonian is fully specified, the total energy of Eq.(1) is used in Monte-Carlo simulations to compute finite-temperature properties of PZT alloys. We use $10 \times 10 \times 10$ supercells (5000 atoms), since this choice yields well-converged results at low temperature[24]. The $\{\sigma_j\}$ variables are chosen randomly in order to mimic maximal compositional disorder, consistent with experimental reality[25], and are kept fixed during the Monte-Carlo simulations. We find that averaging our results over a couple of different realizations of the disorder leads to well-converged statistical properties. The outputs of the Monte-Carlo procedure are the local mode vectors $\mathbf{u}$ and the homogeneous strain tensor η_H. We use the correlation-function approach of Refs 13,14 to derive the piezoelectric and dielectric response from these Monte-carlo simulations. Up to 10^6 Monte-Carlo sweeps are first performed to equilibrate the system, and then 2×10^4 sweeps are used to get the various statistical averages. In the present study, the temperature is kept fixed at 50 K. Note that Refs. 4,24 demonstrate that our approach leads to a (converged) theoretical Curie temperature $T_{c,theo}$ of 1032 K for $Pb(Zr_{0.5}Ti_{0.5})O_3$, which is much higher than the experimental value $T_{c,exp}$ of 640 K[26]. This difficulty of reproducing T_c seems to be a general feature of the effective-Hamiltonian approach[8,10,11], and may be due to higher perturbative terms not included in the analytical expression for the total energy. When comparing with measurements, this shortcoming can be overcome by multiplying the temperature used in the simulation by a constant factor of $T_{c,exp}/T_{c,theo}$[4,13]. As a result, our simulated temperature of 50 K corresponds to an "experimental" temperature around 30 K.

III. RESULTS

A. Structural properties

The averaged homogeneous strain variables obtained in $Pb(Zr_{1-x}Ti_x)O_3$ from our simulations are shown in Fig. 1 as a function of the composition x. These strain variables are measured relative to the LDA-calculated minimum-energy cubic structure with lattice constant a_0 = 7.56 a.u., and are expressed in the Voigt notation. For Ti compositions larger than 49%, we have $\eta_1 = \eta_2 \neq 0$, $\eta_3 > \eta_2$, and $\eta_4 = \eta_5 = \eta_6 = 0$. This strain tensor corresponds to a tetragonal phase with 5 atoms per unit cell. For compositions lower than 47.5%, we predict that the system adopts the so-called "high-temperature"

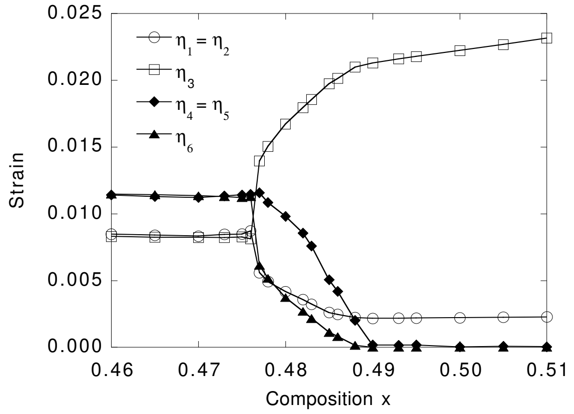

FIG. 1. The average homogeneous strain tensor η_H as a function of composition in disordered $Pb(Zr_{1-x}Ti_x)O_3$ at 50 K. Strains are measured relative to the theoretical minimum-energy cubic structure of lattice constant 7.56 a.u.

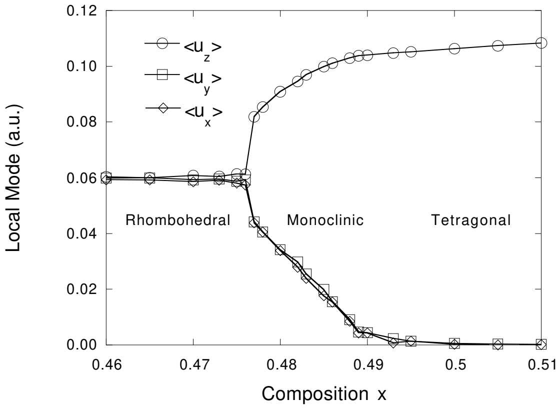

FIG. 2. Average cartesian coordinates $\langle u_x \rangle$, $\langle u_y \rangle$ and $\langle u_z \rangle$ of the local-mode vector as a function of composition x in disordered $Pb(Zr_{1-x}Ti_x)O_3$ at 50 K, corresponding to an experimental T=30 K after rescaling (see text).

(5-atoms per unit cell) rhombohedral phase[27] since $\eta_1 = \eta_2 = \eta_3 \neq 0$ and $\eta_4 = \eta_5 = \eta_6 \neq 0$. The most interesting feature of Fig. 1 is the behavior of the homogeneous strain for the compositional range between 47.5% and 49%: as x decreases, (1) η_1 and η_2 slightly increase and remain equal to each other, (2) η_3 strongly decreases but is still larger than η_1, (3) η_4 and η_5 increase and are equal to each other, and (4) η_6 increases and is smaller than η_4. This behavior is characteristic of an intermediate phase that is neither tetragonal nor rhombohedral, but rather is monoclinic. From the strain tensor shown in Fig. 1, we further predict that this monoclinic phase can be characterized by a 10-atom conventional cell (5-atom primitive cell) with lattice vectors $\mathbf{a}_m = a_0(-1 - \eta_1 - \eta_6/2, -1 - \eta_1 - \eta_6/2, -\eta_4)$, $\mathbf{b}_m = a_0(1+\eta_1-\eta_6/2, -1-\eta_1+\eta_6/2, 0)$, and $\mathbf{c}_m = a_0(\eta_4/2, \eta_4/2, 1 + \eta_3)$. These predictions are in excellent quantitative agreement with the lattice vectors of the monoclinic phase experimentally discovered by Noheda *et al.*[2]. Fig 1 also reveals that the strain variables continuously change with composition when crossing the tetragonal–to–monoclinic transition, while these variables exhibit a sudden jump at the monoclinic–to–rhombohedral transition composition. Interestingly, these two distinct features are consistent with the predictions of Ref. 28, i.e., that the tetragonal–to–monoclinic transition is of second order while the monoclinic–to–rhombohedral transition is of first-order.

Our simulations also agree with measurements for the narrowing of the compositional range of the monoclinic phase when increasing the temperature[3]. For instance, Fig. 1 indicates that the monoclinic phase is predicted to occur for $0.475 < x < 0.49$ at T=50 K, while we predict (not shown here) that increasing the simulated temperature up to 485K – which corresponds to an experimental temperature of 300 K – leads to the existence of the monoclinic phase for $0.475 < x < 0.485$. As observed in Ref. 3, the tetragonal–to–monoclinic transition composition thus decreases when increasing temperature while the rhombohedral–to–monoclinic transition concentration is independent of the temperature. Unfortunately, the calculations are not sufficiently precise to determine whether the phase diagram of PZT exhibits a triple point where the rhombohedral, monoclinic and tetragonal phases meet at a given composition and temperature as suggested in Ref. 29, or whether the monoclinic phase instead survives right up to the boundary with the paraelectric cubic phase. Furthermore, Ref. 29 reports that, at T=20 K, the monoclinic phase is observed for $0.46 < x < 0.51$, i.e. for a larger range that the one shown in Fig. 1. This may be explained by our empirical finding that the range of the monoclinic phase depends strongly on the parameters of Eq. (3). A slight adjustment of these parameters may thus lead to a better agreement with experiment for the compositional range of the monoclinic phase. Note also that our model cannot predict the so-called "low-temperature" rhombohedral phase[27] since this involves oxygen octahedra-tilting degrees of freedom that are not including in the present model. Consequently, our simulations demonstrate that the oxygen tilts are not the driving force for the transition or for the occurrence of the monoclinic phase.

Figure 2 shows the cartesian coordinates ($\langle u_x \rangle$, $\langle u_y \rangle$ and $\langle u_z \rangle$) of the supercell average of the local mode vectors in $Pb(Zr_{1-x}Ti_x)O_3$ as a function of the composition x at $T = 50\ K$, as predicted by our approach described by Eqs. (1) and (2). The average local mode $\langle \mathbf{u} \rangle$, and hence the polarization, is parallel to the pseudo-cubic [001] direction in the tetragonal phase ($x > 0.49\%$) while the polarization becomes parallel to the pseudo-cubic [111] direction in the rhombohedral phase ($x < 0.475\%$). In the monoclinic phase, the change of strain shown in Fig. 1 is associated with a decrease of $\langle u_z \rangle$ while $\langle u_x \rangle$ and $\langle u_y \rangle$ increase and remain nearly equal to each other as the composition x decreases from 49% to 47.5%. Figure 2 thus demonstrates that the electrical polarization rotates from the pseudo-cubic [001] direction to the the pseudo-

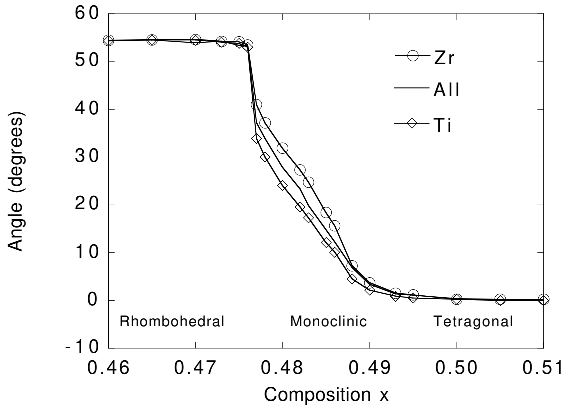

FIG. 3. Angle between the average local-mode vector and the pseudo-cubic [001] direction as a function of composition in disordered $Pb(Zr_{1-x}Ti_x)O_3$ at 50 K. Circles and diamonds refer to averages over local modes centered on Zr and Ti sites, respectively; solid line refers to average over all local modes.

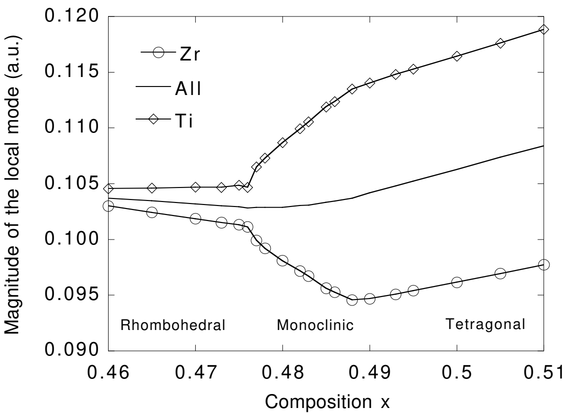

FIG. 4. Magnitude of the average local-mode vector as a function of composition in disordered $Pb(Zr_{1-x}Ti_x)O_3$ at 50 K. Circles and diamonds refer to averages over local modes centered on Zr and Ti sites, respectively; solid line refers to average over all local modes.

cubic [111] direction as the Ti composition decreases in this monoclinic phase.

To better understand the separate contribution of Zr and Ti atoms to this rotation, Fig. 3 shows the composition dependence of the angle δ between the pseudo-cubic [001] direction and the $\mathbf{u}_{\rm Zr}$ (respectively, $\mathbf{u}_{\rm Ti}$) local mode vectors averaged over cells centered on Zr (respectively, Ti) atoms. The angle between the pseudo-cubic [001] direction and the entire supercell average $\langle \mathbf{u} \rangle$ is also shown in Fig. 3. Similarly, Fig. 4 displays the variation of the magnitude of $\langle \mathbf{u} \rangle$, $\mathbf{u}_{\rm Zr}$ and $\mathbf{u}_{\rm Ti}$ as a function of the composition. Figure 3 demonstrates that, in the monoclinic phase, $\mathbf{u}_{\rm Zr}$ and $\mathbf{u}_{\rm Ti}$ also rotate from the [001] direction – for which $\delta = 0$ – to the [111] direction – for which $\delta = 54.7°$ – as the Ti composition decreases from 49% to 47.5%. In this monoclinic phase, the pseudo-cubic [111] direction is always closer to $\mathbf{u}_{\rm Zr}$ than to $\mathbf{u}_{\rm Ti}$. Furthermore, Fig. 4 indicates that the magnitude of $\mathbf{u}_{\rm Zr}$ is smaller than the magnitude of $\mathbf{u}_{\rm Ti}$ in the entire monoclinic phase concentration range, and that the magnitude of $\mathbf{u}_{\rm Zr}$ increases while the magnitude of $\mathbf{u}_{\rm Ti}$ decreases when the Ti composition decreases from 49% to 47.5%. This leads to a nearly composition-independent magnitude of $\langle \mathbf{u} \rangle$. In other words, the total polarization simply rotates in the monoclinic phase while the polarization associated with Zr (respectively, Ti) atoms rotates and also grows (respectively, shrinks), as the Ti concentration decreases.

The authors of Ref. 3 suggested that near the MPB, the rhombohedral and tetragonal phases of PZT can be described in terms of a structure that is locally monoclinic, and in which the average polarization along the [111] or [001] pseudo-cubic direction can occur by means of fluctuations between a subset of three or four nearby monoclinic orientations. In this picture, the transition from the rhombohedral or tetragonal phase to the monoclinic phase would occur by the freezing in of one of these monoclinic orientations. Our effective Hamiltonian can be used to investigate the local structure of PZT around its MPB, and, in particular, to check if the local structure of the tetragonal or rhombohedral phase is different from its average structure. Figures 5(a-c) display the predicted local modes distributions, at T=50 K, for $Pb(Zr_{1-x}Ti_x)O_3$ solid solutions with x=0.50 (tetragonal average structure), x=0.482 (monoclinic average structure) and x=0.47 (rhombohedral average structure), respectively. One can clearly see that the direction and magnitude of the local modes fluctuate around their average value in any of these three PZT solid solutions. As a result, various unit cells adopt a local structure different from the macroscopic average. However, our calculations do not support the hypothesis that the tetragonal and rhombohedral phases of PZT are simply made up of a small number of local monoclinic phases, since Figs. 5(a) and 5(c) do not show the distributions breaking up into clusters centered along the monoclinic directions.

B. Piezoelectric and dielectric properties

We now use our alloy effective Hamiltonian to investigate the piezoelectric and dielectric properties of $Pb(Zr_{1-x}Ti_x)O_3$ *vs.* x at T = 50 K. Figure 6 shows the piezoelectric coefficients d_{33} and d_{15} as a function of the composition x, when representing the piezoelectric tensor in the orthonormal basis formed by $\mathbf{a}_1 = [100]$, $\mathbf{a}_2 = [010]$ and $\mathbf{a}_3 = [001]$. Figure 7 displays the composition dependence of the dielectric susceptibilities χ_{11} and χ_{33} expressed in the same basis.

One can notice that d_{15} is much larger than d_{33} in the tetragonal phase, i.e., for $x > 49\%$. This is consistent with recent measurements revealing that the piezoelectric elongation of the tetragonal unit cell of PZT does not occur along the polar [001] direction[7]. The large value of d_{15} also explains the strong piezoelectric response ob-

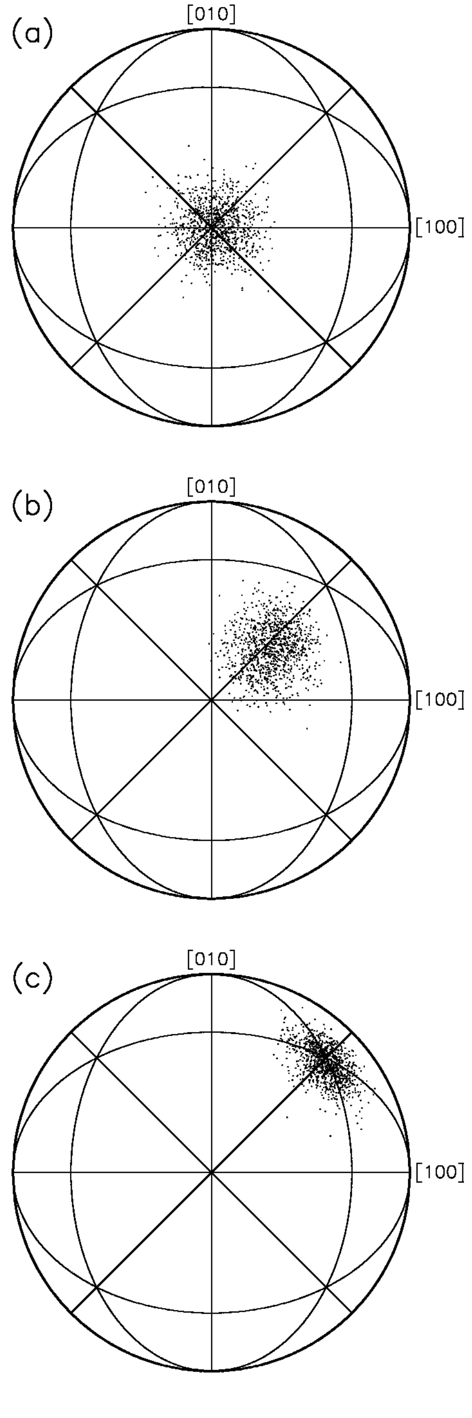

FIG. 5. Projection of the distribution of local-mode orientations for disordered $Pb(Zr_{1-x}Ti_x)O_3$ at 50 K for (a) x=0.50, (b) x=0.482, and (c) x=0.47.

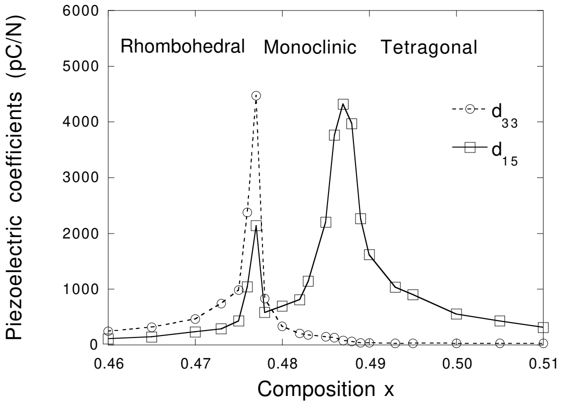

FIG. 6. Piezoelectric coefficients d_{33} and d_{15} as a function of composition in disordered $Pb(Zr_{1-x}Ti_x)O_3$ at 50 K. Statistical errors are estimated to be ~10% of the values displayed.

served in ceramic samples, since this latter involves an average over the single-crystal coefficients d_{15} and d_{33}[4].

One can also see that d_{33} is predicted be quite large in the rhombohedral phase (occurring for $x < 47.5\%$). This prediction agrees with the theoretical and experimental findings of Ref. 30,31 that the d_{33} coefficient of rhombohedral materials can be very large along the [001] direction, i.e. away from the polar direction which is oriented along the pseudo-cubic [111] direction.

Fig. 6 also reveals that d_{33} reaches its largest value near the monoclinic–to–rhombohedral transition, while d_{15} peaks near both the monoclinic–to–rhombohedral and tetragonal–to–monoclinic transitions. The most striking feature of Fig. 6 is that d_{15} has a remarkably large value – above 600 pC/N – in the entire monoclinic phase range.

Fig. 7 demonstrates that the dielectric susceptibility χ_{33} behaves in a similar way as the piezoelectric coefficient d_{33}, in the sense that χ_{33} is also peaked near the monoclinic–to–rhombohedral transition and is also much larger in the rhombohedral phase than in the tetragonal structure. On the other hand, χ_{11} behaves in a manner similar to d_{15}, since they both have peaks at both transitions, and are both very large in the monoclinic phase.

It thus appears that the rotation of the polarization (see Fig. 2) not only leads to a very high d_{15} piezoelectric response (see Fig. 6), consistent with the finding of Ref. 32, but also to a large χ_{11} dielectric response (see Fig. 7).

IV. CONCLUSIONS

In summary, we have used the first-principles derived computational scheme proposed in Ref. 4 to study low-temperature properties of disordered $Pb(Zr_{1-x}Ti_x)O_3$ solid solutions near the MPB.

We find that the monoclinic phase reported in Ref. 2 acts as a structural bridge between the tetragonal phase ($x > 49\%$ at T=50 K) and the rhombohedral phase ($x < 47.5\%$ at T=50 K), with the electric polarization

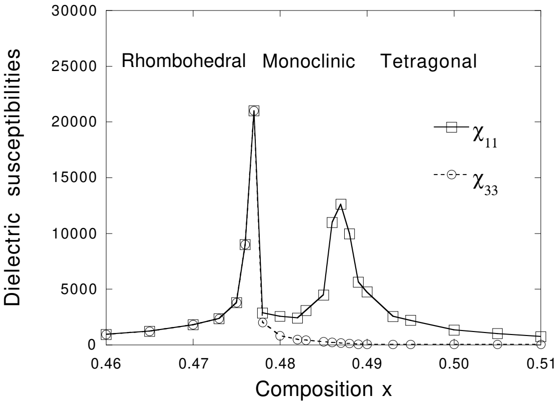

FIG. 7. Dielectric susceptibilities χ_{11} and χ_{33} as a function of composition in disordered $Pb(Zr_{1-x}Ti_x)O_3$ at 50 K. Statistical errors are estimated to be $\sim$10% of the values displayed.

rotating from the pseudo-cubic [001] to [111] direction as the Ti concentration decreases through the monoclinic range. The polarization associated with the Zr atoms differs from the polarization associated with Ti atoms in the monoclinic phase, in that the former rotates faster towards the [111] direction and grows in magnitude, while the latter rotates more slowly and shrinks as the composition x decreases. Furthermore, we also investigated the local structures of tetragonal, monoclinic and rhombohedral PZT alloys, and found that the local polarizations centered in the different unit cells fluctuate significantly in both magnitude and direction around their average value. However, the pattern of these variations does not support a picture in which the tetragonal or rhombohedral phases could be regarded as arising from fluctuations among neighboring monoclinic states. Finally, some piezoelectric and dielectric coefficients are predicted to be extremely large in this monoclinic phase.

V. ACKNOWLEDGMENTS

L.B. thanks the financial assistance provided by the Arkansas Science and Technology Authority (grant N99-B-21), the Office of Naval Research (grant N00014-00-1-0542) and the National Science Foundation (grant DMR-9983678). A.G. acknowledges support from the Spanish Ministry of Education (grant PB98-0244). D.V. acknowledges the financial support of Office of Naval Research grant N00014-97-1-0048. We wish to thank B. Noheda and T. Egami for very useful discussions.

[1] B. Jaffe, W.R. Cook and H. Jaffe, *Piezoelectric ceramics*, (Academic Press, London) (1971).

[2] B. Noheda, D.E. Cox, G. Shirane, J.A. Gonzalo, L.E. Cross, and S-E. Park, *Appl. Phys. Lett.* **74**, 2059 (1999).

[3] B. Noheda, J.A. Gonzalo, L.E. Cross, R. Guo, S-E. Park, D.E. Cox and G. Shirane, *Phys. Rev. B* **61**, 8687 (2000).

[4] L. Bellaiche, A. García and D. Vanderbilt, *Phys. Rev. Lett.* **84**, 5427 (2000).

[5] D.A. Berlincourt, C. Cmolik and H. Jaffe, *Proc IRE* **48**, 220 (1960).

[6] K. Uchino, *Piezoelectric actuators and ultrasonic motors*, (Kluwer Academic Publishers, Boston) (1996).

[7] R. Guo, L.E. Cross, S-E. Park, B. Noheda, D.E. Cox and G. Shirane, *Phys. Rev. Lett.* **84**, 5423 (2000).

[8] W. Zhong, D. Vanderbilt and K.M. Rabe, *Phys. Rev. Lett.* **73**, 1861 (1994); *Phys. Rev. B* **52**, 6301 (1995);

[9] N. Setter and L.E. Cross, *J. Appl. Phys.* **51**, 4356 (1980).

[10] U. Waghmare and K. Rabe, *Phys. Rev. B* **55**, 6161 (1997).

[11] H. Krakauer, R. Yu, C.-Z. Wang and C. LaSota, *Ferroelectrics* **206-207**, 133 (1998).

[12] J. Padilla, W. Zhong and D. Vanderbilt, *Phys. Rev. B* **53**, R5969 (1996). HERE

[13] A. García and D. Vanderbilt, in *First-Principles Calculations for Ferroelectrics: Fifth Williamsburg Workshop*, R.E. Cohen, ed. (AIP, Woodbury, New York, 1998), p. 53.

[14] A. García and D. Vanderbilt, *Appl. Phys. Lett.* **72**, 2981 (1998).

[15] K.M. Rabe and E. Cockayne, in *First-Principles Calculations for Ferroelectrics: Fifth Williamsburg Workshop*, R.E. Cohen, ed. (AIP, Woodbury, New York, 1998), p. 61.

[16] L. Nordheim, *Ann. Phys.* (Leipzig) **9**, 607 (1931).

[17] L. Bellaiche and D. Vanderbilt, *Phys. Rev. B* **61**, 7877 (2000).

[18] N. J. Ramer and A. M. Rappe, *J. Phys. Chem. Solids*, **61**, 317 (2000).

[19] D. Vanderbilt, *Phys. Rev. B* **41**, 7892 (1990).

[20] P. Hohenberg and W. Kohn, *Phys. Rev.* **136**, B864 (1964); W. Kohn and L.J. Sham, *ibid.* **140**, A1133 (1965).

[21] S. de Gironcoli, P. Giannozzi and S. Baroni, *Phys. Rev. Lett.*, **66**, 2116 (1991).

[22] N. Marzari, S. de Gironcoli and S. Baroni, *Phys. Rev. Lett.*, **72**, 4001 (1994).

[23] A.M. Saitta, S. de Gironcoli, and S. Baroni, *Phys. Rev. Lett.* **80**, 4939 (1998).

[24] L. Bellaiche, A. García and D. Vanderbilt, *Proceedings of the 2000 Aspen Winter Conference on Fundamental Physics of Ferroelectrics*, R.E. Cohen, ed. (AIP, Woodbury, New York, 2000), p. 79 (2000).

[25] L.E. Cross, *Ferroelectrics* **151**, 305 (1994).

[26] T. Yamamoto, *Jpn. J. Appl. Phys.* **35**, 5104 (1996).

[27] M.E. Lines and A.M. Glass, *Principles and Applications of Ferroelectrics and Related Materials* (Clarendon Press, Oxford, 1977).

[28] D. Vanderbilt and M.H. Cohen, *cond-mat.*, 0009337 (2000).

[29] B. Noheda, D.E. Cox, G. Shirane, R. Guo, B. Jones and L.E. Cross, *cond-mat.*, 0006152 (2000).

[30] X.-H. Du, J. Zheng, U. Belegundu and K. Uchino, *Appl. Phys. Lett.* **72**, 2421 (1998).

[31] S.-E. Park and T.E. Shrout, *J. Appl. Phys.*, **82**, 1804 (1997).

[32] H. Fu and R.E. Cohen, *Nature* **403**, 281 (2000).